Aerosol Science and Technology
Publication details, including instructions for authors and subscription information:
http://www.tandfonline.com/loi/uast20

Particle Deposition in a Multiple-Path Model of the Human Lung

B. Asgharian, W. Hofmann & R. Bergmann

Version of record first published: 30 Nov 2010

To cite this article: B. Asgharian, W. Hofmann & R. Bergmann (2001): Particle Deposition in a Multiple-Path Model of the Human Lung, Aerosol Science and Technology, 34:4, 332-339

To link to this article: http://dx.doi.org/10.1080/02786820119122

Aerosol Science and Technology 34: 332–339 (2001)

Published by Taylor and Francis
0278-6826/01/$12.00 + .00

Particle Deposition in a Multiple-Path Model of the Human Lung

B. Asgharian,[1] W. Hofmann,[2] and R. Bergmann[2]
[1]*Chemical Industry Institute of Toxicology, Research Triangle Park, North Carolina*
[2]*Institute of Physics and Biophysics, University of Salzburg, Austria*

Predicting the amount of particle deposition in the human lung following exposure to airborne particulate matter is the first step toward evaluating risks associated with exposure to airborne pollutants. Realistic deposition models are needed for accurate predictions of deposition in the lung, but a major limitation is the degree to which the lung geometry can be accurately reconstructed. Morphometric data for the entire airway tree of the human lung are not available. So far, idealistic lung structures have been used for deposition calculations. In this study, 10 statistical lung structures based on morphometric measurements of Raabe et al. (1976) were generated for the conducting airways of the human lung. A symmetric, dichotomous branching alveolar airway structure was attached to the end of the conducting airway tree of each lung structure. The total volume of the alveolar region was the same among the lung geometries. Using a mathematical scheme developed previously (Anjilvel and Asgharian 1995), regional, lobar, and per-generation depositions of particles were calculated in these geometries. The results were compared to deposition predictions using typical-path and five-lobe symmetric lung geometry models. All three lung models showed very similar regional and generation-by-generation deposition results. Lobar deposition was found to strongly depend on the detailed morphometry of the lung structure that was used.

Various deterministic models of particle deposition in the respiratory tract have been formulated to calculate the deposition of inhaled particles in humans and animals. The models range from empirical models that do not incorporate lung geometry (Rudolf et al. 1986, 1990) to mathematically complex, many-path (multiple-path) models that are based on a lung structure constructed from actual airway measurements (Anjilvel and Asgharian 1995; Asgharian and Anjilvel 1998). In addition, a stochastic lung deposition model using statistical relationships of airway parameters to reconstruct the lung geometry has been devised (Koblinger and Hofmann 1985, 1990). Empirical and typical-path lung models are useful for quick calculation of particle deposition but produce limited information. These models are useful for obtaining average regional and overall deposition of particles in the lung. More detailed and site-specific information can be gained by using many-path and stochastic models in which more accurate assessment of the lung structure is included.

A recent study comparing these two models in rats revealed that both models produce similar regional deposition (Hofmann et al. 2000). In the deterministic, multiple-path model of particle deposition, the conducting airways were selected from morphometrical measurements obtained in rats (Raabe et al. 1976). An eight-generation, dichotomous branching, symmetric acinar region proposed by Yeh et al. (1979) was attached to the terminal airways. In the stochastic model, the conducting airways for the first few upper generations were selected from the measurements of Raabe et al. (1976). The remaining airways in the conducting and pulmonary region were reconstructed from frequency distributions (or probability density functions) of airway lengths, diameters, and branching angles that were based on morphometry measurements of Raabe et al. (1976). In rats, interanimal variability is negligible for the conducting airways (Menache et al. 1991) but is significant in the acinar region. For this reason, a hybrid model that used the conducting tree structure of the multiple-path model and the acinar structure of the stochastic model was created and compared to the multiple-path and stochastic models. All three models showed similar deposition in the tracheobronchial region (Hofmann et al. 2000). Thus the differences in alveolar deposition were mainly due to differences in acinar structure.

In humans, there is no comprehensive morphometry data set comprising the entire conducting airways of the lung. Only limited measurements on adult males are available (e.g., Weibel 1963; Horsfield and Cumming 1968; Phalen et al. 1985; Nikiforov and Schlesinger 1985). These models provide only limited information, e.g., average dimensions in all airway generations (Weibel 1963), average values in bronchial airways

Received 17 September 1999; accepted 21 February 2000.
This research was supported in part by CIIT member companies; the Commission of the European Communities, contract FI4P-CT95-0026; and the Jubilaeumsfonds of the Austrian National Bank, project 6325. The authors would also like to thank Dr. Barbara Kuyper for her editorial assistance in the preparation of this manuscript.
Address correspondence to Dr. Bahman Asgharian, Chemical Industry Institute of Toxicology, 6 Davis Drive, P.O. Box 12137, Research Triangle Park, NC 27709-2137. E-mail: asgharian @ciit.org

(Phalen et al. 1985), and average dimensions ± coefficient of variation in large bronchial airways (Nikiforov and Schlesinger 1985). The models are based on symmetric lung structure (Weibel 1963; Phalen et al. 1985; Nikiforov and Schlesinger 1985). Yu and Diu (1982) investigated the effect of lung structure on particle deposition in different airway generations. The lung structures were normalized to the same functional residual capacity (FRC).

Yeh et al. (1979) proposed two geometric structures for the conducting airways: a typical-path symmetric model with dichotomous branching pattern and a five-lobe model. In the five-lobe model, each lobe had a typical-path symmetric and dichotomously branching pattern. However, each lobe had a different structure. The alveolar regions in both lung structures were also assumed to be symmetric and dichotomous branching. Employing the mathematical analogy used for particle deposition in the rat lung (Anjilvel and Asgharian 1995), the two lung data sets were used to create a typical-path and a limited multiple-path model of particle deposition (Subramaniam et al. 2000). The deposition results of the typical-path model were consistent with the previous mathematical models, including the trumpet model (Yu 1978). The regional and overall deposition results were similar for both typical-path and five-lobe symmetric but structurally different models. In addition, the five-lobe symmetric model was capable of predicting lobar and lobar regional deposition. The lobar deposition results indicated that deposition among various lobes can be significantly different. Thus the common practice of using regional deposition predictions from a typical-path model to assess lung response as a result of exposure to airborne pollutants may not be adequate. Some uncertainties regarding the lobar deposition predictions of the five-lobe symmetric model remain since some inconsistencies from the experimental data were observed (Subramaniam et al. 2000).

The use of a five-lobe symmetric structure lung to predict particle deposition represents improvement over the typical-path models currently in wide use. However, the symmetric structure within each lobe poses a limitation on the ability of the model to predict site-specific deposition patterns. Thus a more accurate assessment of the lung structure is needed. Establishing a truly multiple-path model of particle deposition based on an asymmetric lung geometry that matches human airway structure and dimensions closely is highly desirable.

A statistical lung structure was proposed by Koblinger and Hofmann (1985) for humans. Based on morphometric measurements, various statistical probability density functions describing airway parameters were derived for the reconstruction of the human airway tree. The lung geometry has been used in a stochastic model to calculate particle deposition in a stochastically average human lung (Koblinger and Hofmann 1990; Hofmann and Bergmann 1998). In the deposition model, reconstruction of the entire airway tree was avoided by using a Monte-Carlo technique that required the selection of only one pathway at a time for the computation of particle deposition. Deposition fractions were calculated without producing the entire respiratory tract. However, the statistical relationships between airway parameters can feasibly be used to reconstruct the entire airway tree from the distribution functions of the airways. The reconstructed airway tree can then be used in a mathematically deterministic lung deposition model for particle deposition calculations.

Based on the arguments stated above concerning the need for a complete deterministic model of the entire human airway tree and due to impracticality in measuring the entire human airway tree, the available measurements and statistical relationships among various airways employed in the stochastic model were used to construct 10 five-lobe, asymmetric, structurally different human airway trees. These lung structures, combined with the mathematical formulation used in the multiple-path model of particle deposition in rats (Anjilvel and Asgharian 1995), formed a truly multiple-path model of particle deposition in humans. The model was used to calculate the deposition of inhaled particles in different regions, lobes, and each generation of the human lung. The calculated results were compared against the deposition results obtained using the typical-path and five-lobe symmetric-path lung geometries.

DESCRIPTION OF THE LUNG GEOMETRY

Different lung structures were used here for particle deposition calculation. However, these different lungs were all based on the same morphometric measurements (Raabe et al. 1976). The lung structures referred to an adult, healthy, and nonsmoking male person.

Yeh et al. (1979) used morphometrical measurements of Raabe et al. (1976) for a single human cast to create a symmetric, dichotomous branching, typical-path and a five-lobe symmetric but structurally different lung geometry. These simplified geometries are employed here to calculate particle deposition.

A stochastic morphometric model of the human lung was used (Koblinger and Hofmann 1990) to construct a tracheobronchial tree describing the randomness and asymmetry of the airway branching system. The lung model is based on distributions of morphometric parameters such as length, diameter, branching angle, cross-sectional area of the daughter tubes, gravity angle, and correlations between these parameters as a function of airway generation (Koblinger and Hofmann 1985). In the morphometric model used in the earlier developed deposition model, the lung geometry in a specific generation is based on a series of random selections for every generation. In the present model, in contrast, each airway tube is based on a single selection from the individual parameter distributions. For this reason, the construction of one tracheobronchial tree represents the bronchial tree of an individual person rather than a population-averaged lung. However, several calculations with different selections from the distributions can be performed to simulate the lungs of individual subjects and to illustrate intersubject variability. Ten such geometries were constructed here

for the conducting region of the lung. These lungs were based on the same structural relationships, varying primarily in their lung volumes. These lungs were examined visually by plotting them three dimensionally. They resembled realistic lung structures of humans. Slight underestimation of intersubject variability in human population may result from the use of these lungs provided that structural differences affect particle deposition.

Sufficient morphometric measurements are not available to reconstruct the entire alveolar region. Based on theoretical considerations, Yeh et al. (1979) reconstructed a regular dichotomous alveolar branching structure regarding the number and dimensions of alveolar airways that were used in their typical-path model. The human bronchial tree in the current model was supplemented by attaching identical alveolar regions of Yeh et al. (1979) to the end of each terminal bronchiole. The terminal airways provided the root tree for each alveolar acinus. The structure of the alveolar region was similar to the last seven generations of the typical-path model of Yeh et al. (1979) for humans. The length, diameter, and branching pattern of the alveolar ducts in the current stochastic lungs remained the same as those in the Yeh et al. (1979) model. Since the numbers of terminal airways in the typical-path and stochastic lungs were different, so were the numbers of alveolar regions ($2^{16} = 65{,}536$ in the Yeh et al. model and 20,285–54,093 in the stochastically-generated lungs). The dimensions of the alveolar sacs in the stochastic lungs were adjusted such that the total alveolar volume remained the same in all the lungs. Thus each alveolar volume in each stochastic lung was $2^{16}/N$ times the alveolar volume of that of Yeh et al. (1979), where N is the number of terminal airways of that stochastic lung. The alveoli were distributed among the seven generations of the pulmonary region in the same proportions as those in the Yeh et al. (1979) model. The airway measurements of Yeh et al. (1979) were made at total lung capacity. In the current study, the airway length and diameter were scaled down to a FRC of 3300 ml in all the lungs. During respiration, the airways were assumed to expand and contract uniformly. Thus the airway dimensions at a given tidal volume (V_T) were further normalized to FRC + $V_T/2$.

PARTICLE DEPOSITION MODEL

The symmetric typical-path or five-lobe symmetric lung structures of Yeh et al. (1979) are simplified assumptions of a more general asymmetric lung geometry. The same mathematical formalism for particle deposition was used to calculate deposition in all lung geometries. The flow in each airway was assumed to be proportional to its distal volume. The details of the mathematical formalism used to calculate particle deposition in the rat lung are given elsewhere (Anjilvel and Asgharian 1995; Asgharian and Anjilvel 1998).

Particle deposition in different regions of the lung was calculated for unit density particles ranging from 0.01 to 10 μm in diameter. Deposition fractions were calculated for a functional residual capacity of 3300 ml, a tidal volume of 625 ml, and a breathing frequency of 12 breaths per minute (minute ventilation = 7500 ml). Particles were assumed to enter the lung via an endotracheal tube (i.e., there was no upper respiratory tract volume). A breathing frequency of 12 breaths per minute with equal breathing time during inhalation and exhalation was assumed. No pause between inhalation and exhalation was used.

RESULTS AND DISCUSSION

Total Deposition Fraction

The deposition fractions of particles ranging from 0.01 to 10 μm in diameter in the entire lung, tracheobronchial, and alveolar regions are shown in Figures 1 through 3, respectively, for the typical-path, five-lobe symmetric, and stochastic lung geometries. Ten stochastic lung geometries were generated, and the deposition fraction in each was found. The mean deposition fractions ± standard deviation of the deposition fractions for the 10 lung geometries were calculated and plotted in the figures. The overall deposition fraction for the three lung structures is shown in Figure 1. The five-lobe symmetric and stochastic lung geometries predicted similar deposition results that were slightly lower than that of typical-path lung model. The predicted deposition fraction line of five-lobe symmetric lung fell within the standard deviation of the stochastic lung deposition fractions, indicating that these two geometries essentially predicted the same deposition fractions. Since all three lung geometries produced similar overall deposition fraction when assessing total deposition fraction, any model can be used for prediction. In the tracheobronchial region (Figure 2), similar findings were also

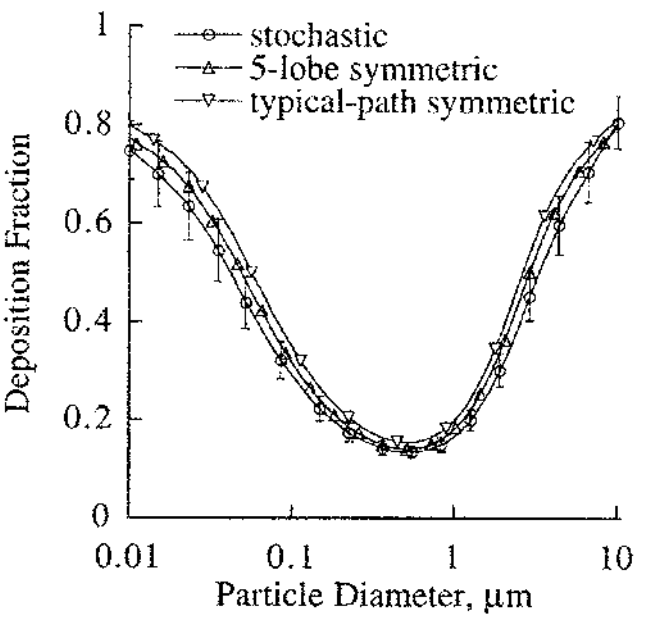

Figure 1. Total deposition fraction of unit density particles in the three lung geometries for various particle diameters. Lung functional residual capacity was 3300 ml, and minute ventilation was 7500 ml.

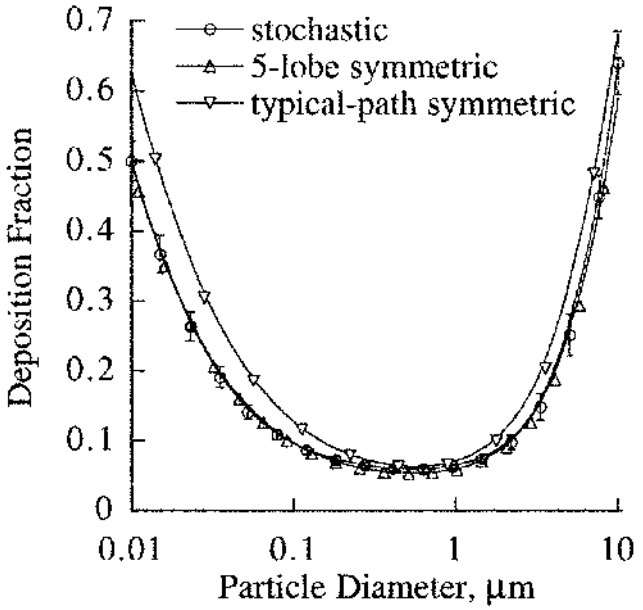

Figure 2. Tracheobronchial deposition fraction of unit density particles in the three lung geometries for various particle diameters. Lung functional residual capacity was 3300 ml, and minute ventilation was 7500 ml.

observed. Both lobar models gave similar deposition fraction predictions that were slightly lower than those for the typical-path model. Deposition fraction in the alveolar region is shown in Figure 3 for all lung geometries. Deposition fraction in the alveolar region of the stochastic model showed greater variation in deposition than that in the tracheobronchial region, mainly due to differences in number and volume of individual alveolar regions in various stochastically generated lungs. Deposition curves for the typical-path and five-lobe symmetric lungs fell within the standard deviation of the deposition fraction in the stochastic lungs. Thus deposition fractions in all three lungs were statistically the same.

Deposition Fraction Per Generation

All three lung models are capable of predicting deposition fraction per airway generation, but, since the typical-path and five-lobe symmetric lungs are based on average lung geometry, the deposition results for these two cases should be considered as average per generation. Deposition per airway generation for the three lung geometries are calculated for particles of 0.01, 1, and 10 μm. The deposition fraction of 0.01 μm particles per airway generation for all three lungs is shown in Figure 4. Deposition fraction in the stochastic lung model is represented by mean deposition fraction $\pm$ standard deviation (SD). Since diffusion is the dominant loss mechanism for 0.01 μm particles, most deposition occurs in the lower airway generations. The typical-path and five-lobe symmetric lungs show similar results since both lung models are based on symmetric lung structures. The stochastic lung has more airway generations and, consequently, particle deposition is more distributed in the later generations compared with the other two models. While little variation in deposition was observed in the early airway generations of the stochastic lung, there was significant variation in the later generations, possibly due to differences in the alveolar regions of the stochastic lung geometries. The results suggest that when

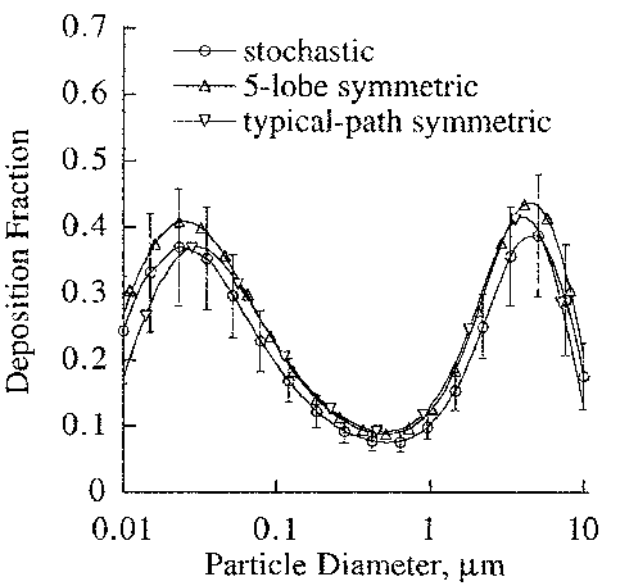

Figure 3. Alveolar deposition fraction of unit density particles in the three lung geometries for various particle diameters. Lung functional residual capacity was 3300 ml, and minute ventilation was 7500 ml.

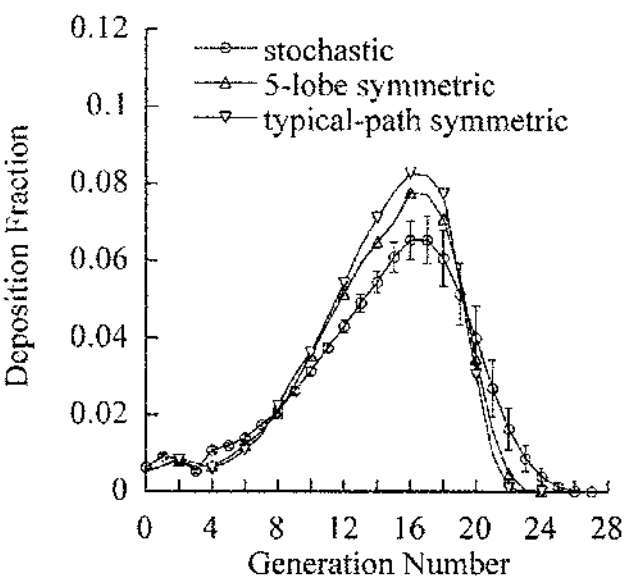

Figure 4. Deposition fraction of 0.01 μm unit density particles in the three lung geometries as a function of airway generation number. Lung functional residual capacity was 3300 ml, and minute ventilation was 7500 ml.

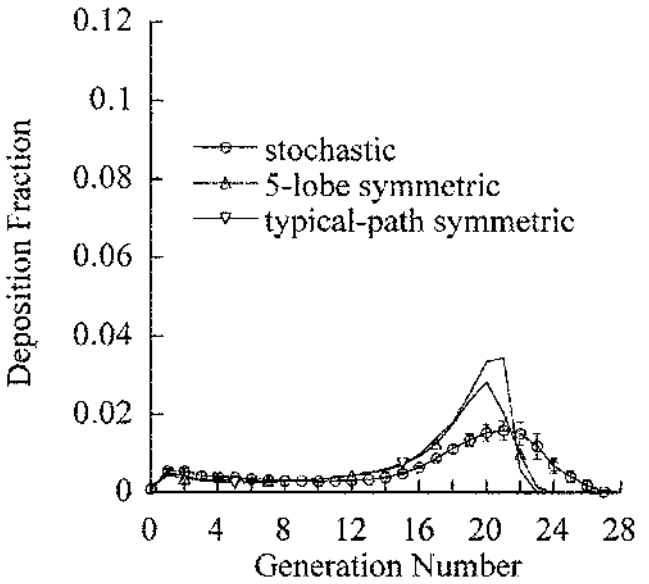

Figure 5. Deposition fraction of 1 μm unit density particles in the three lung geometries as a function of airway generation number. Lung functional residual capacity was 3300 ml, and minute ventilation was 7500 ml.

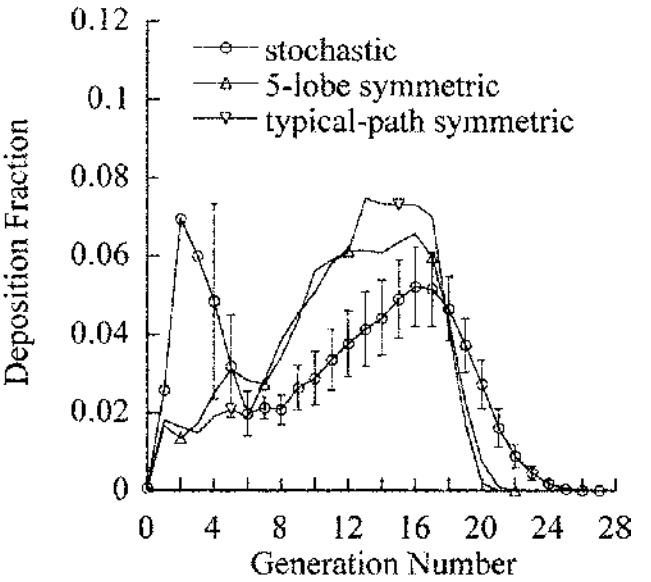

Figure 6. Deposition fraction of 10 μm unit density particles in the three lung geometries as a function of airway generation number. Lung functional residual capacity was 3300 ml, and minute ventilation was 7500 ml.

diffusion is the dominant loss mechanism, the main difference in deposition among different models is due to differences in generation number rather than airway dimensions.

The generation-by-generation deposition fraction of 1 μm particles deposited for each of the three lung structures is shown in Figure 5. The results show similar patterns as in the previous case, even though loss mechanisms in the lower airways are due to sedimentation and diffusion combined. Variation of deposition in the stochastic model was quite small. All three models showed similar deposition fractions in the upper airways. Due to an increased number of airway generations, the stochastic lung showed more dispersed and thus lower deposition than the other two symmetric lung models.

A different pattern was observed when deposition of 10 μm particles per generation was calculated. Stochastic lungs exhibited much different deposition fractions in the first few upper airway generations from those in the two symmetric lungs (Figure 6). The standard deviation of the deposition fraction was quite large. For this reason, the error bars for the first four generations are not shown. This large variation of deposition among the stochastic lungs is mainly due to differences in airway dimension and orientation. Losses in these airways are by impaction. Thus impaction losses are strongly dependent on geometry.

Deposition fraction in the succeeding airways, where impaction was no longer present and sedimentation was the dominant loss mechanism, is similar to the previous two cases. Due to an increased number of airway generations, losses in the stochastic lungs are more distributed and thus lower than those in the other two lungs.

Lobar Deposition Fraction

As far as regional or even generation-by-generation results are concerned, any of these models can be used to predict particle losses in the lung. However, a more elaborate lung structure is needed if further detailed deposition results are required.

As mentioned earlier, 10 stochastic lung geometries were generated for deposition calculations. These geometries varied in dimensions and generation number to encompass various possible geometries of human adult lungs. Each geometry yielded different deposition results. Deposition fractions in all five lobes of each of the stochastic lung geometries were calculated. The results are presented in Figures 7a–7e. The figures show the range of deposition values as a function of particle diameter. Variation in lobar deposition was more pronounced at small and large particle sizes and varied by a factor of 3.

Total lobar deposition per lobe in the five-lobe symmetric lung is reported in Figure 8. The results show that corresponding lobes in the left and right lungs produced almost identical results (e.g., deposition fraction in the right upper lobe was the same as that in the left upper lobe, and deposition in the right lower lobe was the same as that in the left lower lobe). Furthermore, lower lobes yielded the highest deposition fractions followed by the upper lobes and then the right middle lobe. Tracheobronchial and pulmonary deposition in each lobe (not shown) also showed the same trend.

The total mean lobar deposition for the 10 stochastic lung models that were generated is shown in Figure 9. Some similarities exist between these results and those for the five-lobe symmetric model, but the differences outweigh the similarities. In the five-lobe symmetric lung geometry, corresponding lobes in the left and right lung gave almost identical deposition fraction

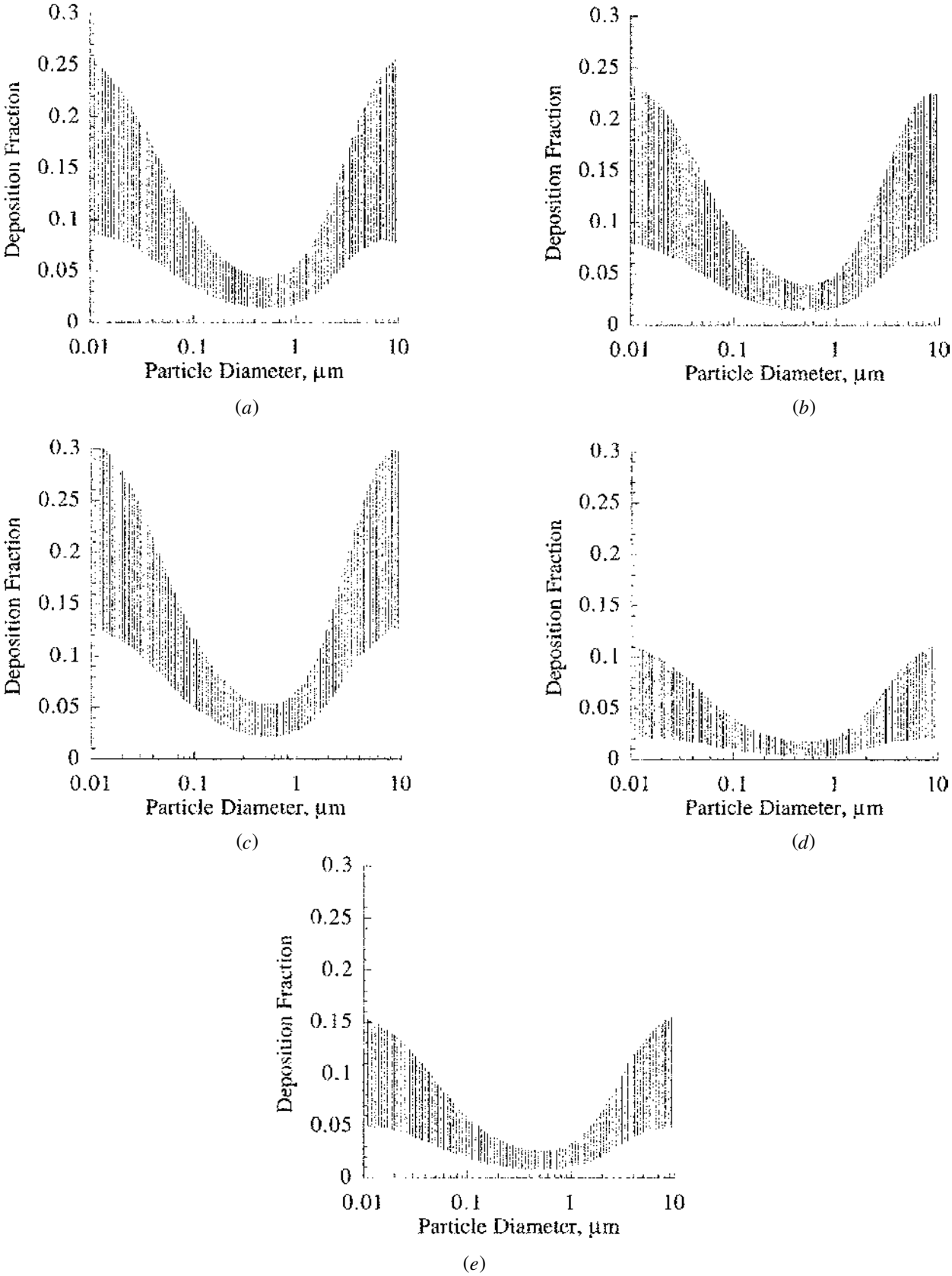

Figure 7. Range of total lobar deposition fractions of unit density particles in 10 separate stochastic lung geometries for various particle diameters. Lung functional residual capacity was 3300 ml, and minute ventilation was 7500 ml. (a) Left upper lobe, LU; (b) left lower lobe, LL; (c) right upper lobe, RU; (d) right middle lobe, RM; and (e) right lower lobe, RL.

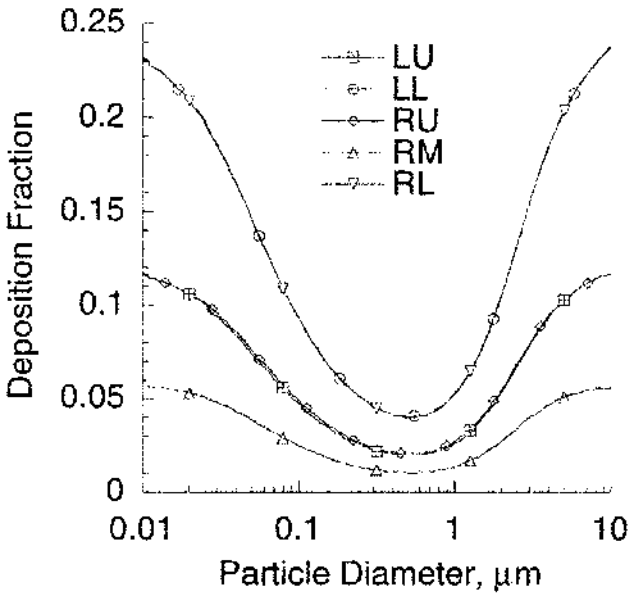

Figure 8. Total lobar deposition fraction of unit density particles in the five-lobe symmetric lung geometry for various particle diameters. Lung functional residual capacity was 3300 ml, and minute ventilation was 7500 ml. Left upper lobe, LU; left lower lobe, LL; right upper lobe, RU; right middle lobe, RM; right lower lobe, RL.

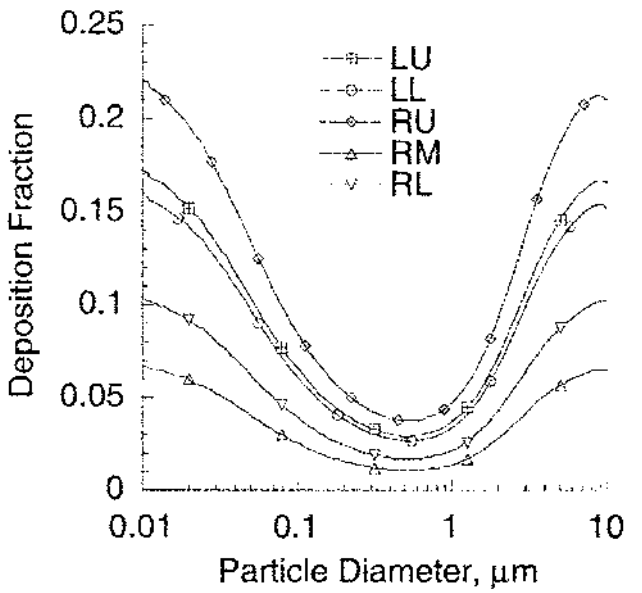

Figure 9. Total mean lobar deposition fractions of unit density particles in stochastic lung geometry for various particle diameters. Lung functional residual capacity was 3300 ml, and minute ventilation was 7500 ml. Left upper lobe, LU; left lower lobe, LL; right upper lobe, RU; right middle lobe, RM; right lower lobe, RL.

results (Figure 7). This is believed to be due to symmetric lobe structures. In the stochastic models, although the same lobar trend of deposition is observed, the corresponding lobes had very different deposition values. Furthermore, deposition in the lower left lobe was only slightly smaller than that in the left upper lobe. The right middle lobe and right lower lobe had the smallest deposition values. If the deposition fractions of these two lobes are added, values similar to those for the left lower lobe are obtained.

A comparison of Figures 7 and 9 shows that lobar deposition is different in the two models. Furthermore, the location of the highest and the lowest deposition fraction is also opposite in the two models. A preliminary comparison suggests a better comparison of the experimental data with the results of the stochastic model. Thus detailed airway morphometry is critical for determination of site-specific deposition even though it may not be necessary for regional deposition calculations.

There are many alveolar acini in each of the stochastic lung geometries. The initiation of lung injury in these regions is most likely directly related to the initial deposition of particles. Not all alveolar regions receive the same dose. To examine regional variation of alveolar deposition in more detail, the deposition fraction in each alveolar region was computed for a stochastic lung geometry having 21,553 terminal bronchioles. This resulted in 21,553 alveolar deposition fractions that together form the alveolar deposition fraction distribution. The alveolar deposition fraction distributions for particle sizes 0.01, 0.1, 1, and 10 μm are plotted in Figure 10. A point on each curve corresponds to the number of alveolar acini indicated by the ordinate

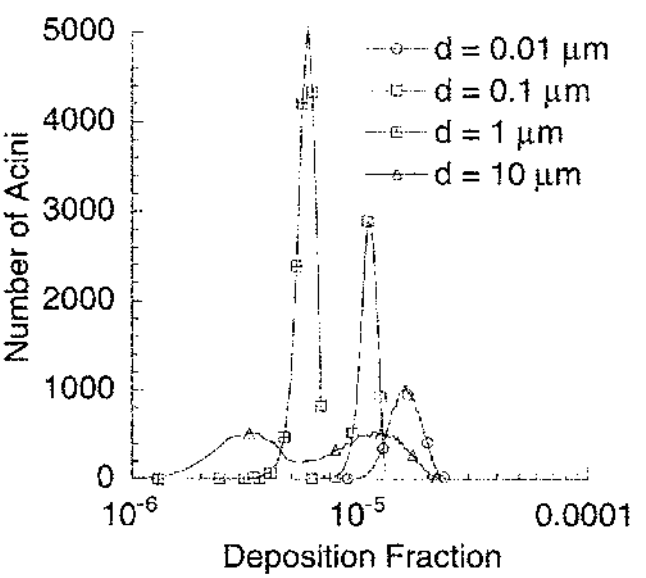

Figure 10. Alveolar deposition fraction distribution for four different particle sizes. Particle mass density was 1 g/cm^3, lung functional residual capacity was 3300 ml, and minute ventilation was 7500 ml.

value having a deposition fraction between $X - 3 \times 10^{-7}$ and X, where X is the corresponding abscissa value. The results show a narrow distribution for 0.01, 0.1, and 1 μm particles, indicating that the alveolar acini received similar deposition of these sized particles. On the other hand, a wide distribution with two peaks was observed for 10 μm particles. This means that significant differences in deposition fractions exist among various alveolar regions.

The fractional depositions of particles in the human lung were presented using three lung geometries: typical-path symmetric, five-lobe symmetric, structurally different, and five-lobe asymmetric (stochastic). Due to a lack of sufficient airway measurements, idealized airway structures were used for the alveolar region. The alveolar size and volume was assumed to be the same for each region extending past any given terminal bronchioles, which is a highly simplified assumption that influences final deposition results. Any model improvement has to include a better assessment of this region.

CONCLUSIONS

Deposition fractions of particles in different models of the human respiratory tract were calculated. Lung geometries used in the study included a typical-path model, five-lobe symmetric but structurally different model, and 10 stochastic lung models illustrating intersubject variability among the human population. Deposition fraction in the tracheabronchial region, pulmonary region, and entire respiratory tract was found to be statistically the same when any of the above models was employed. Differences in average deposition per generation for the 10 stochastic lungs were found to be small, reflecting primarily differences in linear airway dimensions among these geometries. However, deposition among individual airways in a given generation varied significantly as a result of intersubject variability in lung morphology at the single airway level. These results were significantly different in the lower airway generations from those found using typical-path or five-lobe models. Lobar deposition was found to be significantly different between the five-lobe model and the stochastic lungs. A variation in deposition fraction of up to three folds was observed among various stochastic lungs, indicating that various individuals may receive different doses in each lobe.

REFERENCES

Anjilvel, S., and Asgharian, B. (1995). A multiple-path model of particle deposition in the rat lung, *Fundam. Appl. Toxicol.* 28:41–50.

Asgharian, B., and Anjilvel, S. (1998). A multiple-path model of fiber deposition in the rat lung, *Toxicol. Sci.* 44:80–86.

Hofmann, W., Asgharian, B., Bergmann, R., Anjilvel, S., and Miller, F. J. (2000). The effect of heterogeneity of lung structure on acinar particle deposition in the rat lung, *Toxicol. Sci.*, in press.

Hofmann, W., and Bergmann, R. (1998). Predictions of particle deposition patterns in human and rat airways, *Inhal. Toxicol.* 10:557–583.

Horsfield, K., and Cumming, G. (1968). Morphology of the bronchial tree in man, *J. Appli. Physiol.* 24, 373–383.

Koblinger, L., and Hofmann, W. (1985). Analysis of human lung morphometric data for stochastic aerosol deposition calculations, *Phys. Med. Biol.* 30:541–556.

Koblinger, L., and Hofmann, W. (1988). Stochastic morphological model of the rat lung, *Anat. Rec.* 221:553–539.

Koblinger, L., and Hofmann, W. (1990). Monte Carlo modeling of aerosol deposition in human lungs. Part I: Simulation of particle transport in a stochastic lung structure, *J. Aerosol Sci.* 21:661–674.

Koblinger, L., and Hofmann, W. (1995). Aerosol inhalation in the rat lung. Part II: Theoretical predictions of particle deposition patterns, *J. Aerosol Med.* 8:21–32.

Menache, M. G., Patra, A. L., and Miller, F. J. (1991). Airway structure variability in the Long-Evans rat lung, *Neurosci. Biobehav. Rev.* 15:63–69.

Nikiforov, A. I., and Schlesinger, R. B. (1985). Morphometric variability of the human upper bronchial tree, *Respi. Physiol.* 59:289–299.

Phalen, R. F., Oldham, M. J., Beaucage, C. B., Crocker, T. T., and Mortenson, J. D. (1985). Postnatal enlargement of human tracheobronchial airways and implications for particle deposition, *Anat. Rec.* 212:368–380.

Raabe, O. G., Yeh, H.-C., Schum, G. M., and Phalen, R. F. (1976). Tracheobronchial Geometry: Human, Dog, Rat, Hamster—A Compilation of Selected Data from the Project Respiratory Tract Deposition Models, Report LF-53. Lovelace Foundation, Albuquerque, NM.

Rudolf, G., Gebhart, J., Heyder, J., Schiller, Ch. F., and Stahlhofen, W. (1986). An empirical formula describing aerosol deposition in man for any particle Size, *J. Aerosol Sci.* 17:350–355.

Rudolf, G., Kobrich, R., and Stahlofen, W. (1990). Modelling and algebraic formulation of regional aerosol deposition in man, *J. Aerosol Sci.* 21 (suppl. 1.):S403–S406.

Subramaniam, R., Anjilvel, S., Asgharian, B., and Freijer, J. I. (2000). Analysis of lobar differences in particle deposition in the human lung, in preparation.

Yeh, H. C., Schum, G. T. M., and Duggan, M. T. (1979). Anatomic models of the tracheobronchial and pulmonary regions of the rat, *Anat. Rec.* 195:483–492.

Yu, C. P. (1978). Exact analysis of aerosol deposition during steady breathing, *Powder Technol.* 21:55–62.

Yu, C. P., and Diu, C. K. (1982). A comparative study of aerosol deposition in different lung models, *Am. Ind. Hyg. Assoc. J.* 43:54–65.

Weibel, E. R. (1963). *Morphometry of the Human Lung*, Academic Press, New York.